An Assessment of Entropy-Based Data Reduction for SEI Within IoT Applications

Mohamed A. Taha*, Mohamed K. M. Fadul, Joshua H. Tyler†, Donald R. Reising, and T. Daniel Loveless
The University of Tennessee at Chattanooga
Chattanooga, TN 37403, USA
Email: {rbx441*, ygm111†}@mocs.utc.edu, {mohammed-fadul, donald-reising, daniel-loveless}@utc.edu

***Abstract*—The research community remains focused on addressing Internet of Things (IoT) security concerns due to its continued proliferation and use of weak or no encryption. Specific Emitter Identification (SEI) has been introduced to combat this security vulnerability. Recently, Deep Learning (DL) has been leveraged to accelerate SEI using the signals' Time-Frequency (TF) representation. While TF representations improve DL-based SEI accuracy–over raw signal learning–these transforms generate large amounts of data that is computationally expensive to store and process by the DL network. This study investigates the use of entropy-based data reduction applied to "tiles" selected from the signals' TF representations. Our results show that entropy-based data reduction lowers the average SEI performance by as little as 0.86% while compressing the memory and training time requirements by as much as 92.65% and 80.7%, respectively.**

***Index Terms*—Deep Learning, Time-Frequency Representation, Specific Emitter Identification, Entropy, Feature Extraction.**

I. Introduction

THE Internet of Things (IoT) is formed by connecting inexpensive, semi-autonomous devices–that sense and conduct actions in the physical world–to the Internet [1]. IoT continues to receive a lot of attention within the research community due to its proliferation [2] and weak or nonexistent security [3]–[5]. Specific Emitter Identification (SEI) is a physical layer approach proposed to address these IoT security concerns, because it has been shown capable of discriminating a radio–from others within a set–by exploiting unique and inherent features that are imparted upon its signals during their formation and transmission. The exploited signal features are attributed to the components, sub-systems, and systems that comprise the radio's Radio Frequency (RF) front-end. SEI is a viable IoT security solution for the following reasons. First, SEI exploited signal features do not impede communications system function (i.e., demodulation). Second, published works have shown that SEI is capable of achieving serial number discrimination–which is the most challenging case–as well as an ability to reject devices that change their digital identities (e.g., media access control address, international mobile equipment identity) to circumvent traditional network security approaches (e.g., media access control address filtering) [6], [7]. Third, the exploited features persist over time, location, and environments. Lastly, SEI exploited signal features are generated during the transmitter's normal operation without the need for external stimuli; thus, eliminating the need for IoT device modification(s) and challenges of implementing and managing encryption at scale.

Over the past twenty-five plus years, SEI has primarily used feature engineering (a.k.a., handcrafted features) and traditional Machine Learning (ML) approaches (e.g., support vector machines, random forest, etc.), which rely heavily upon the knowledge and expertise of the person or persons designing the SEI process. Recently, Deep Learning (DL) has received a lot of attention within the SEI community due to its demonstrated success within the fields of: spectrum management [8], [9], modulation identification [10], and system design [10]–[14]. Additionally, DL thrives under increasing amounts of information and can learn transmitter discriminating features directly from the signals' In-phase and Quadrature (IQ) samples [11], [15], [16]. However, the removal of expert involvement is not necessarily advantageous, because its integration can improve DL performance. The work in [10] introduces the Radio Transformer Network (RTN), which integrates expert defined correction algorithms within a DL-based receiver to improve demodulation performance. Expert knowledge is also used in [17] to perform multipath channel correction prior to DL-based SEI, because without it SEI performance is reduced to 9%. Thus, the work in [17] sets a precedent for the integration of expert knowledge within DL-based SEI processes.

Our DL-based approach is motivated by the work in [18], which uses entropy and a Convolutional Neural Network (CNN) to determine if a painting is a forgery or not. Differentiating a forgery–from the legitimate painting–is analogous to differentiating two radios of the same manufacture and model (i.e., serial number discrimination), because a forged painting requires a trained eye to detect it as a forgery and in some cases that is not enough. In [18], a painting's high-resolution image is too large to be processed by a standard CNN, so it is broken into "tiles" and the high entropy tiles–relative to the entire image's entropy–are retained. In ML parlance, the entropy approach in [18] is a data reduction technique and its success led to our investigation into its use within the CNN-based SEI process presented herein. In addition to entropy, we also investigate the use of "enhanced" entropy, which combines entropy with either the mean, standard deviation, variance, skewness, or kurtosis. Our selection of these statistics is based upon our prior SEI publications [7], [19]–[21].

In this paper, we present a DL-based SEI approach that employs entropy to reduce the amount of data stored by IoT

devices or the associated infrastructure. The contributions of our work are as follows:

- The signal transformation is selected based upon our knowledge of the wireless standard employed by the IoT devices. In this case, a Time-Frequency (TF) representation generated from the Gabor Transform's (GT) magnitude response.
- In addition to entropy-driven data reduction, "enhanced" entropy data reduction is introduced and assessed. Statistically driven data reduction is optimized by coupling the entropy with either the mean or kurtosis.
- The presented approach is compared with the more common DL-based SEI approach that learns the radio discriminating features directly from the signals' raw IQ samples.

The presented approach allows the amount of data and training time to be reduced by as much as 92.65% and 80.7%, respectively. Entropy-based data reduction lowers SEI performance by only 0.86% (i.e., average SEI performance is 98.45% using the entire GT derived image versus 97.59% when using the image's entropy selected tiles).

The rest of the paper is organized as follows: Related works are summarized in Sect. II; Sect. III covers the signal of interest as well as the Gabor Transform calculation; Sect. IV discusses signal collection, detection, and post-processing, signal preparation prior to DL, as well as the configurations utilized to build and train the CNN. Results and analysis of our SEI approach are presented in Sect. V, which is followed by the conclusion in Sect. VI.

II. Related Works

The authors in [22] use entropy to select the most relevant features prior to K-Nearest Neighbor (KNN) classification. The features are the spectral components comprising the Random Access CHannel (RACH) preambles emitted by Universal Mobile Telecommunications System (UMTS) radios. The authors in [22] perform SEI using "spectrally averaged" RACH preambles, which combines multiple preambles–emitted by the same radio–together to improve the Signal-to-Noise Ratio (SNR). Our work performs SEI using individual signals (i.e., without averaging). For each spectral component, the entropy is computed across the RACH preambles emitted by a given radio as well as all radios. An individual radio's RACH preamble spectral component is selected if its entropy value is greater than or equal to the entropy value corresponding with the same spectral component but calculated across all radios' RACH preambles. The work in [22] performs traditional SEI under the assumption that the radios can be sufficiently differentiated using only the RACH preambles' entropy-selected spectral components. Thus, entropy is used for feature selection and not data reduction. Our work uses entropy to facilitate the latter in an attempt to minimize the amount of data stored by an IoT device or infrastructure while suffering minimal or no SEI performance degradation. This is achieved by our use of DL-based SEI, which maximizes radio discrimination by learning an optimal feature set. The authors also collect all of the RACH preambles in an anechoic chamber and do not assess their SEI process under degrading SNR conditions. All of the signals used in our work are collected within a traditional laboratory environment; thus, there is interference and other channel impairments present within the collections. We also assess our SEI process for degrading SNR channel conditions.

The authors in [23] improve SEI performance through the use of non-linear, dynamic features. One of these features is designated as the Multi-dimensional Approximate Entropy (MApEn) feature. Computational complexity is reduced through the use of a sliding window and computing MApEn over each window. Overlapping windows are permitted. SEI is performed using a KNN classifier. The work in [23] shows MApEn is a feature with distinct information to enable SEI. Our work also uses a sliding window to partition each signal's representation; however, non-overlapping windows are used to maximize data reduction.

In [24], the authors perform SEI using the bispectrums' color moments. Specifically, the authors introduce the Bispectrum-based method using Energy Entropy and Color Moments (BEECM) to measure the bispectrum's evenness. The color moment determines the similarity between multiple grayscale images based on the intensity information distribution. SEI is performed using Support Vector Machines (SVM). Entropy is used as an SEI feature in [24] while our work uses entropy for data reduction and not as a feature.

III. Background

This section describes the signal of interest as well as the Gabor Transform.

A. Signal of Interest

SEI is performed using features learned from the preamble portion of the IEEE 802.11a Wireless-Fidelity (Wi-Fi) frame. IEEE 802.11a Wi-Fi is an Orthogonal Frequency Division Multiplexing (OFDM) signal whose radios operate in the 5 GHz Industrial, Scientific, and Medical (ISM) band and can achieve data rates up to 54 Megabits-per-second. Every IEEE 802.11a Wi-Fi frame begins with a 16 μs long preamble that is constructed using a set of known, fixed OFDM symbol sequences. These symbol sequences are used by an 802.11a Wi-Fi receiver to perform signal detection, channel equalization, as well as frequency and phase offset correction [25]. The structure of the IEEE 802.11a Wi-Fi preamble is shown in Fig. 1 and consists of ten–designated t_1 through t_{10}–Short Training Symbols (STS), a Guard Interval (GI), and two–designated T_1 and T_2–Long Training symbols (LTS).

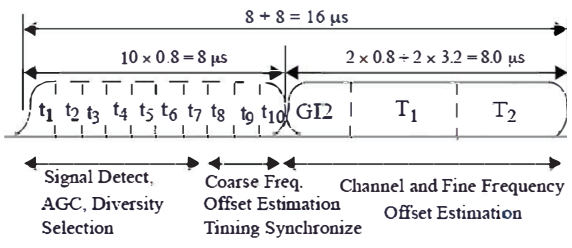

Fig. 1. IEEE 802.11a Wi-Fi preamble structure that comprises the first 16 μs of a frame [25].

Our use of IEEE 802.11a Wi-Fi is for the following reasons: (i) a preponderance of published SEI works use this signal [15], [17], [20], [21], [26], [27], (ii) it is one of the most widely deployed wireless communication standards [17], (iii) it is an IoT designated communications protocol [28], (iv) OFDM is the basis for other current and emerging wireless communications standards such as: Long Term Evolution (LTE), Worldwide Interoperability for Microwave Access (WiMAX), IEEE 802.11ac, IEEE 802.11ad, and IEEE 802.11ax [29], and (v) an on-hand set of compliant radios.

B. Gabor Transform

The Gabor Transform (GT) provides a signal's Time-Frequency (TF) representation and is similar to the Short Time Fourier Transform (STFT) in which a Gaussian window replaces the STFT's rectangular window. Our use of the GT is motivated by the fact that IEEE 802.11a Wi-Fi signals contain fifty-two, time-varying sub-carriers, which makes the signal ideally suited for TF representation. The TF representation ensures that momentary and localized TF variations are jointly captured, which would be otherwise undiscovered–or at least unverifiable–by the CNN. For the results in Sect. V, an IEEE 802.11a Wi-Fi preamble's TF representation is generated using the Discrete GT (DGT), which is calculated by [30],

$$G_{mk} = \sum_{n=1}^{MN_\Delta} s(n)W^*(n - mN_\Delta)exp^{-j2\pi kn/K_G}, \quad (1)$$

where G_{mk} are the Gabor coefficients, $s(n)$=$s(n+lMN_\Delta)$ is the periodic input signal, $W(n)$=$W(n+lMN_\Delta)$ is the periodic analysis window, N_Δ is the total number of shifted samples, m=$1, 2, \ldots, M$ for M total shifts, k=$1, 2, \ldots, K_G - 1$ for $K_G \geq N_\Delta$, and $mod(MN_\Delta, K_G)$=0 satisfied. If $K_G > N_\Delta$, then the GT is said to be "oversampled" and is desirable when processing noisy data. Thus, the oversampled GT is used here to improve SEI performances under degraded SNR conditions. The reader is directed to [30] for more details on the DGT calculation. SEI is conducted using the normalized, magnitude Gabor coefficients [31],

$$\overline{|G_{mk}|} = \frac{|G_{mk}| - min\{|G_{mk}|\}}{max\{|G_{mk}|\} - min\{|G_{mk}|\}}. \quad (2)$$

IV. Methodology

This section explains signal collection, detection, and post-processing; how the signal data set is prepared prior CNN training and testing; the DL configuration and the specifications for the computer used to generate all of the results.

A. Signal Collection, Detection, and Post-Processing

Signals transmitted by eight TP-Link Archer T3-U USB Wi-Fi dongles are collected using a USRP B210 Software-Defined Radio (SDR) at a sampling rate of 40 MHz. Signal detection begins by removing the channel noise present between individual transmissions. Preamble detection and selection is conducted by sliding a window–that is the same length as the preamble–along the transmission's magnitude representation and then calculating the Mean Square Error (MSE) between it and the magnitude of an ideal (i.e., a signal not corrupted by the channel or hardware imperfections) preamble. The magnitude is used to improve preamble detection accuracy, because it is not impacted by the presence of Carrier Frequency Offset (CFO). The window associated with the smallest MSE value is designated as the one containing the preamble. The corresponding complex-valued IQ samples are then removed from the transmission and stored. The detection process is repeated until a total of 10,000 preambles are detected for each radio. Every preamble is then (i) downsampled to 20 MHz, (ii) corrected for CFO [32], as well as (iii) filtered using a fourth-order, lowpass Elliptic filter with a 8.865 MHz cutoff frequency as well as a passband and stopband attenuation of 0.5 dB and 20 dB, respectively. All preambles are normalized to unit energy in accordance with [27].

B. Data Preparation

For the results presented in Sect. V, a specific SNR is achieved by adding scaled and like-filtered Additive White Gaussian Noise (AWGN) to each preamble, which can be expressed as,

$$r(n) = s(n) + \eta\ w(n), \quad (3)$$

where $s(n)$ is the preamble, $w(n)$ is the noise, and η is the scale factor applied to $w(n)$ to achieve the desired SNR value. This process is repeated ten times for each preamble to facilitate Monte Carlo simulation at the selected SNR. SEI performance is assessed using SNR values ranging from 9 dB to 30 dB in increments of 3 dB. The GT is then calculated using (1) with M=320, K_G=320, and N_Δ=1. The result is a 320×320 TF representation of the selected IEEE 802.11a Wi-Fi preamble.

As in [18], we use Claude Shannon's definition of entropy and calculate it in accordance with [33]. Each preamble's normalized, magnitude-squared GT representation is converted to a grayscale image with pixel values ranging from 0 to 255. Each grayscale image is then divided by 255 to ensure its pixel intensities are in the range of zero to one. The entropy is calculated for each resulting normalized, grayscale image [33],

$$\epsilon(I) = -\sum_{j=0}^{255} f_I[j]\log(f_I[j]), \quad (4)$$

where j is a pixel's intensity and $f_I[j]$ is the probability that a given pixel intensity level is within the image-normalized magnitude-squared GT representation I, taken from the Probability Mass Function (PMF) of random variable I. The entropy of a normalized, grayscale image is designated as the "image entropy", $\epsilon_i(I)$. After calculating $\epsilon_i(I)$, the image is subdivided into N_t non-overlapping tiles and entropy calculated for each tile. The entropy of tile t is denoted as $\epsilon_i^t(I)$. If the tile entropy satisfies,

$$\epsilon_i^t(I) \geq \epsilon_i(I), \quad (5)$$

then the tile is retained for subsequent SEI processing; otherwise, it is discarded. In addition to entropy-based data reduction, data reduction is also performed using "enhanced"

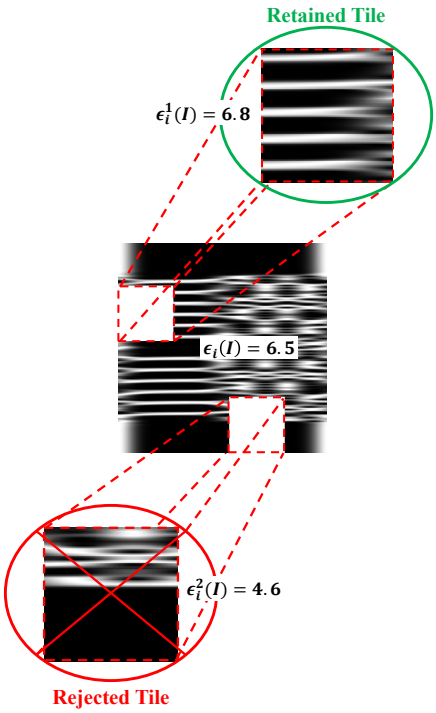

Fig. 2. Representative illustration showing a case where the tile above the image would be retained due to its $\epsilon_i^1(I)$=6.8 entropy being greater than the $\epsilon_i(I)$=6.5 entropy of the entire image. The other tile–whose $\epsilon_i^2(I)$=4.6 entropy is less than $\epsilon_i(I)$=6.5–would be rejected.

entropy. The enhanced entropy approach uses entropy and another statistic to select the tiles used for SEI. The additional statistics investigated are: mean μ, standard deviation σ, variance σ^2, skewness γ, and kurtosis κ [34]. In enhanced entropy, a tile's entropy and selected statistic values must be equal to or greater than the image's entropy and selected statistical value. For example, if the additional statistic is kurtosis, then equation (6) must be satisfied in addition to equation (5) for the tile to be retained for later SEI processing.

$$\kappa_i^t(I) \geq \kappa_i(I), \tag{6}$$

where $\kappa_i^t(I)$ is the kurtosis calculated over tile t of image I and $\kappa_i(I)$ is the kurtosis calculated over the entire image I. Fig. 2 provides a representative illustration of the tile selection process. In this example, the $\epsilon_1^t(I)$=6.8 entropy of the tile located above the IEEE 802.11a Wi-Fi preamble's TF image would be retained for subsequent SEI classification. While the tile–whose entropy is $\epsilon_2^t(I)$=4.8–would be rejected.

Tile sizes of: 100×100, 125×125, 130×130, and 135×135 are used in this work. Other tile sizes (e.g., 50×50) were investigated, but neither selection process (i.e., entropy and enhanced entropy) resulted in any retained tiles for at least one radio within the set of eight. This prevents identification of that radio using the presented approach; thus, the other investigated tiles sizes are omitted. It is important to note that the developed tile selection process can result in a different number of retained tiles per radio; thus, the radio represented by the fewest number of retained tiles sets the number of retained tiles used to represent the remaining radios. In this case, the tiles are uniformly selected. Table I presents the minimum number of tiles obtained using the entropy and enhanced entropy tile retention approaches for each of the four tile sizes at an SNR of 30 dB.

TABLE I
THE NUMBER OF TILES RETAINED USING THRESHOLDS DEFINED BY THE ENTROPY (ϵ) OR ENHANCED ENTROPY FOR ONE OF FOUR TILE SIZES AT AN SNR OF 30 DB. ENTROPY IS ENHANCED USING THE MEAN (μ), STANDARD DEVIATION (σ), VARIANCE (σ^2), SKEWNESS (γ), OR KURTOSIS (κ).

Tile Size	ϵ	ϵ & μ	ϵ & σ	ϵ & σ^2	ϵ & γ	ϵ & κ
100x100	19,458	14,453	7,400	7,400	3,392	505
125x125	4,583	4,583	32	32	0	898
130x130	3,187	3,187	12	12	0	267
135x135	4,874	4,874	1	1	0	815

C. Deep Learning Configuration

For the results in Sect. V, the CNN consists of four layers with a total of: eight, eight, sixteen, and thirty-two filters per layer, respectively. All filters are set to a size of 35×35. For a given SNR and noise realization, the CNN is trained by randomly assigning 90% of the retained tiles to the training set and the remaining 10% used for "blind" testing. The blind test set classification results are presented in Sect. V. The CNN training process integrates k=10-fold cross-validation to achieve a more generalized model [35]. The error performance is tracked for each fold within a noise realization as well as across noise realizations. The CNN model which achieves the smallest average error–across all folds and noise realizations–is designated as the "best" model and used to classify the retained tiles' blind test set at the corresponding SNR.

D. Computer Specifications

All results are generated using MATLAB® R2020b [36] running on a high performance computational cluster consisting of four compute nodes. Each node is comprised of two Intel Xeon Gold 6148 CPUs, four NVIDIA Tesla 32 GB V100s running driver version 450.80.02 and Cuda SDK version 11.0, 192 GB of error correction code RAM, and running 64-bit Redhat Linux release 8.3.2011.

V. RESULTS

Initial SEI assessment focuses on determining the tile sizes and entropy-based data reduction approach that results in the highest average percent correct classification performance at an SNR of 30 dB. The associated results are shown in Table II. It is important to note that Table II entries of "–" denote the case in which an insufficient number of retained tiles are available to train the CNN (see Table I). Table II shows that using entropy (ϵ), entropy & mean (ϵ & μ) or entropy & kurtosis (ϵ & κ) results in an average percent correct classification performance above 97% when selecting tiles of size 135×135. Based upon the results in Table II, individual SEI performance is presented using confusion matrices for the 135×135 sized tiles selected using ϵ, ϵ & μ, or ϵ & κ, Fig. 3.

TABLE II
AVERAGE PERCENT CORRECT CLASSIFICATION PERFORMANCE FOR ALL FOUR TILE SIZES THAT ARE RETAINED BASED UPON THE ENTROPY OR ENHANCE ENTROPY AT AN SNR OF 30 DB. TABLE ENTRIES OF "–" CORRESPOND TO CASES IN WHICH THERE IS NOT ENOUGH TILES TO TRAIN THE CNN.

Tile Size	ϵ	ϵ & μ	ϵ & σ	ϵ & σ^2	ϵ & γ	ϵ & κ
100x100	92.68%	92.98%	90.93%	91.15%	94.92%	87.83%
125x125	93.88%	93.88%	--	--	--	95.60%
130x130	94.74%	95.80%	--	--	--	94.57%
135x135	**97.59%**	**97.92%**	--	--	--	**97.24%**

Fig. 3(a) presents individual radio percent correct classification performance when the CNN is trained and tested using the entire 320×320 sized, GT-based images. In this case, statistical data reduction is *not* performed; thus, the normalized images are used in their entirety. These results serve as a baseline against which the results in Fig. 3(b), Fig. 3(c), and Fig. 3(d) are compared. In terms of individual percent correct classification, SEI performance remains consistent (i.e., it is above 95%) for all radios regardless of the statistical method used to determine which 135×135 tiles are retained or rejected. In fact, the average percent correct classification performance is only 0.86%, 0.76%, and 1.21% lower when using 135×135 tiles selected via ϵ (Fig. 3(b)), ϵ & μ (Fig. 3(c)), and ϵ & κ (Fig. 3(d)), respectively. Thus, the difference in SEI performance is negligible when using the reduced data sets in lieu of the entire image set. Table III provides two additional comparisons versus the full, 320×320 GT image case. The amount of memory needed to store the ϵ, ϵ & μ, and ϵ & κ selected data sets is greatly reduced by as much as 92.8%, 91.3%, and 98.5% versus the full, 320×320 GT image data set, respectively. A reduced data size corresponds to faster CNN training, which is beneficial for cases in which the CNN needs to be re-trained due to changes in the IoT infrastructure (e.g., a device is replaced, removed, or added).

A. Results: SNR Performance Analysis

Based upon the presented SEI results, an additional assessment is conducted under degrading SNR conditions. Average percent correct classification performance is presented for GT image tiles selected using the ϵ, ϵ & μ, and ϵ & κ approaches for SNR values ranging from 9 dB to 30 dB in 3 dB increments, Fig. 4 and Table V. Table IV provides the number of tiles used to generate the results in Fig. 4 and Table V at each SNR. In addition to the entropy-based data reduced results, SEI results are presented for the case when

TABLE III
AMOUNT OF MEMORY NEEDED TO STORE THE FULL, 320×320 GT IMAGE DATA SET AND THE TIME NEEDED TO TRAIN ITS CNN FOR A SINGLE NOISE REALIZATION ACROSS ALL TEN CROSS-VALIDATION FOLDS AT SNR OF 30 DB VERSUS THE 135×135 TILES. THE NUMBERS IN PARENTHESES DENOTE THE PERCENT REDUCTION WITH RESPECT TO THE 320×320 GT IMAGE CASE.

	Full Image	ϵ	ϵ & μ	ϵ & κ
Memory in Gigabytes	65.54	4.73 (92.8%)	5.73 (91.3%)	0.97 (98.5%)
Time in Minutes	418.02	80.6 (80.7%)	97.73 (76.6%)	18.9 (95.5%)

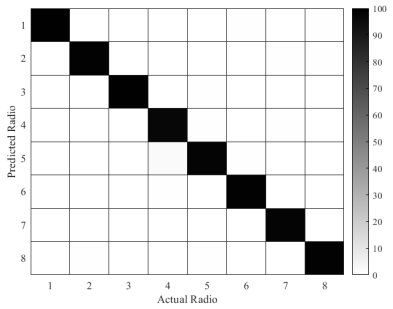

(a) Full, 320×320 GT images (i.e., no data reduction) with an average accuracy 98.45%.

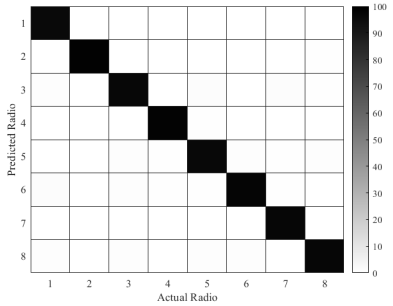

(b) Entropy only with an average accuracy of 97.59%.

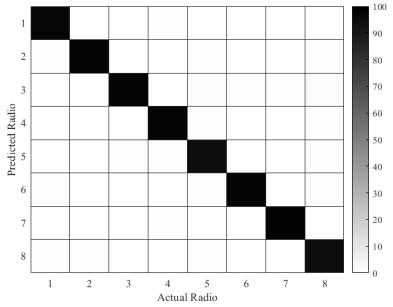

(c) Entropy & mean with an average accuracy of 97.92%.

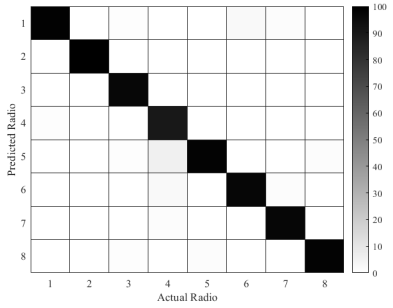

(d) Entropy & kurtosis with an average accuracy of 97.24%.

Fig. 3. Confusion matrices showing percent correct classification of the eight IEEE 802.11a Wi-Fi radios associated with the three highest average percent correct values–for 135×135 tiles–in Table II at an SNR of 30 dB.

the CNN is trained and tested using the IEEE 802.11a Wi-Fi preambles' raw IQ samples–collected for each radio–and their derived 320×320, grayscale GT images. The IQ-based results are included to facilitate comparative assessment with current state-of-the art DL-based SEI approaches. While the full, 320×320, grayscale GT image-based results serve as a baseline against which the data reduced results are compared. GT tiles selected using only the ϵ are superior to the IQ-based results for SNRs of 12 dB and higher and are comparable to the ϵ & μ results for SNRs of 15 dB and higher. For SNR values of 15 dB and higher, the ϵ & μ retained GT image tiles result in superior SEI performance over the IQ-based results. Average percent correct classification results are presented for SNR values of 24 dB and higher when using ϵ & κ to select the retained GT image tiles, because at lower SNR values none of the 135×135 tiles satisfied their corresponding images' entropy $\epsilon_i(I)$ and kurtosis $\kappa_i(I)$ criteria. The IQ-based SEI results are superior to all data reduced cases when the SNR is 9 dB; however, this is at the expense of a training time in excess of 180 minutes and higher memory requirements. The full, 320×320, grayscale GT image-based results are superior to the IQ-based results and only slightly better than the entropy-based results for SNRs of 18 dB and higher. The full GT images' superior SEI performance shows the benefit of expert knowledge. The entropy reduced data sets' lower SEI performance is attributed to the fact that fewer tiles are retained as SNR degrades, Table IV. Fewer tiles are retained, because more of the entropy dependent information–present in the preambles' grayscale images–is obscured as the noise power increases. However, this trend reverses at 9 dB. This is attributed to the noise power beginning to influence the image, $\epsilon_i(I)$, and tile, $\epsilon_i^t(I)$, entropy values, which results in more tiles meeting or exceeding the selection threshold.

The entropy-based SEI performance–at lower SNRs–may be improved by using: (i) RGB images instead of grayscale.

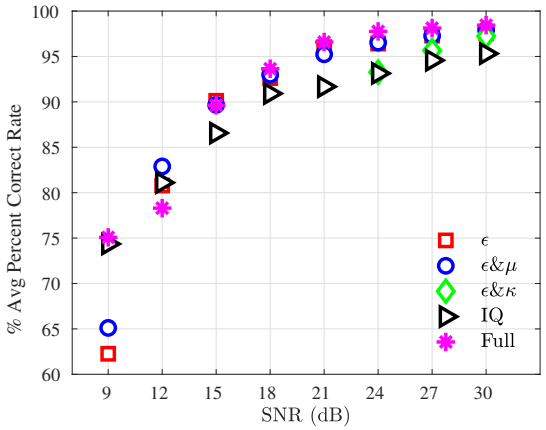

Fig. 4. Average percent correct classification performance for 135×135 GT derived tiles that are selected for further SEI processing using entropy (ϵ), entropy & mean (ϵ & μ) or entropy & kurtosis (ϵ & κ) at SNR values of 9 dB to 30 dB in steps of 3 dB. The "IQ" designated results are generated by training and testing a CNN using only the IEEE 802.11a Wi-Fi preambles' complex-valued IQ samples. The "Full" designated results correspond to CNN training and testing using the full, 320×320 grayscale GT images.

TABLE IV
THE NUMBER OF 135×135 ENTROPY (ϵ), ENTROPY & MEAN (ϵ & μ), OR ENTROPY & KURTOSIS (ϵ & κ) SELECTED TILES USED TO GENERATE THE RESULTS IN FIG. 4.

	9 dB	12 dB	15 dB	18 dB	21 dB	24 dB	27 dB	30 dB
ϵ	786	217	398	870	1,667	2,785	3,940	4,874
ϵ & μ	747	197	397	870	1,667	2,785	3,940	4,874
ϵ & κ	140	5	2	7	48	260	518	815

The RGB images could lead to a three-fold increase in the number of tiles available for SEI exploitation. This would lead to increased training times and memory requirements; (ii) a tile size optimized for lower SNRs, a range of SNRs, or each SNR. Our approach selected the tile size based upon average percent correct classification achieved at an SNR of 30 dB, which may not be an optimal tile size for lower SNRs; (iii) a deeper CNN; or (iv) data augmentation [37]. Our results are generated using a four layer CNN, which is technically a deep NN, but it is far from being as deep as the NNs used in other SEI publications [17]. In our case, the limited number of tiles (e.g., 786 at 9 dB) prohibits training and updating of deeper networks, because as network depth increases so does the number of parameters. As the number of parameters increases more time and data is needed to train the network to prevent overfitting. Use of one, two, or all of these alternative approaches will depend upon the IoT application, which will require a balance to be struck between SEI performance and the resources (i.e., memory, computational capacity, power, etc.) available and needed to achieve it.

In addition to the average percent correct classification results presented in Fig. 4 and Table V, the confusion matrices in Fig. 5 show individual radio SEI performance generated using ϵ as well as ϵ & μ retained tiles for the four lowest SNR values (i.e., 9 dB through 18 dB). Fig. 5(a), Fig. 5(c), Fig. 5(e), and Fig. 5(g) are the confusion matrices for the ϵ retained tiles at the SNRs of 9 dB, 12 dB, 15 dB, and 18 dB, respectively. The confusion matrices for ϵ & μ retained tile results are presented in Fig. 5(b), Fig. 5(d), Fig. 5(f), and Fig. 5(h) for SNRs of 9 dB, 12 dB, 15 dB, and 18 dB, respectively. For SNR values of 9 dB, 12 dB, and 18 dB, the ϵ & μ tile selection approach proves superior in that fewer misclassifications occur (i.e., the off-diagonal entries of the confusion matrices are less populated). At 15 dB, the ϵ retained tiles achieved higher average percent correct classification performance. Overall, the performance differences between the ϵ and ϵ & μ approaches are marginal and within the statistical variability of the experiments.

TABLE V
AVERAGE PERCENT CORRECT CLASSIFICATION ACCURACY USING THE 135×135 ENTROPY (ϵ), ENTROPY & MEAN (ϵ & μ), OR ENTROPY & KURTOSIS (ϵ & κ) SELECTED TILES CORRESPONDING TO THE ENTRIES IN TABLE. IV AND SHOWN IN FIG. 4.

	9 dB	12 dB	15 dB	18 dB	21 dB	24 dB	27 dB	30 dB
ϵ	62.26%	80.79%	**90.12%**	92.62%	96.03%	96.42%	97.29%	97.59%
ϵ & μ	65.11%	**82.89%**	89.67%	92.99%	95.24%	96.53%	97.28%	97.92%
ϵ & κ	46.43%	0%	0%	0%	0%	93.27%	95.65%	97.24%
Full	**75.08%**	78.30%	89.63%	**93.65%**	**96.59%**	**97.76%**	**98.13%**	**98.45%**

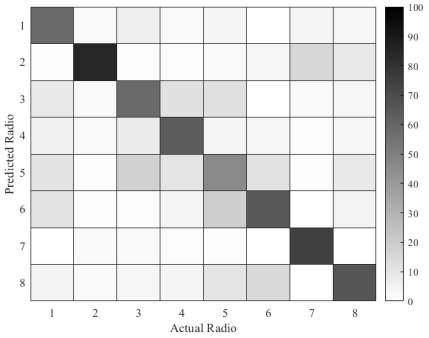

(a) SNR of 9 dB with an average accuracy of 64.81%.

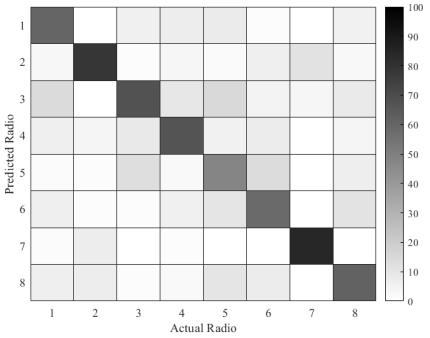

(b) SNR of 9 dB with an average accuracy of 65.11%.

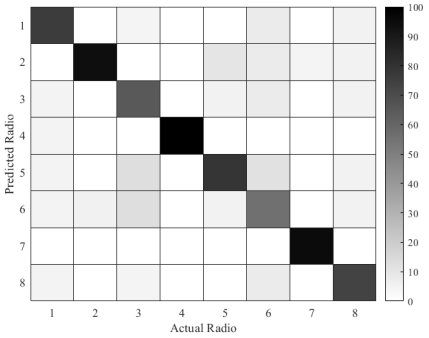

(c) SNR of 12 dB with an average accuracy of 80.79%.

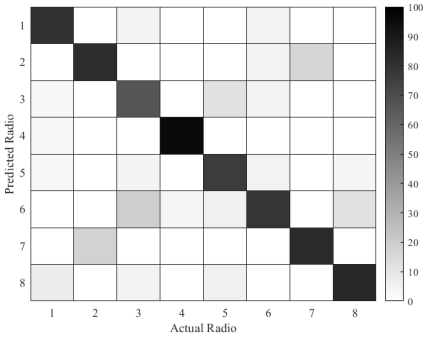

(d) SNR of 12 dB with an average accuracy of 82.89%.

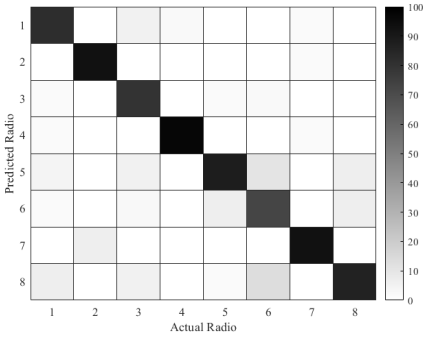

(e) SNR of 15 dB with an average accuracy of 90.12%.

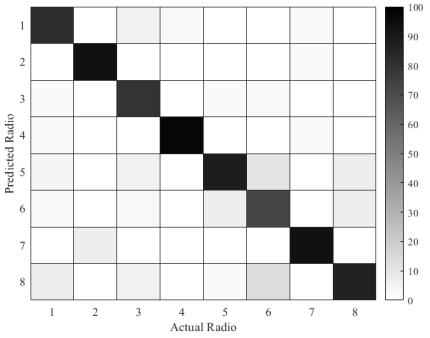

(f) SNR of 15 dB with an average accuracy of 89.67%.

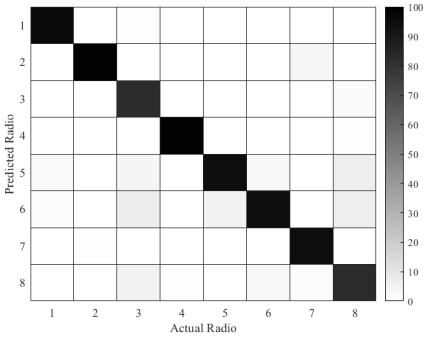

(g) SNR of 18 dB with an average accuracy of 92.62%.

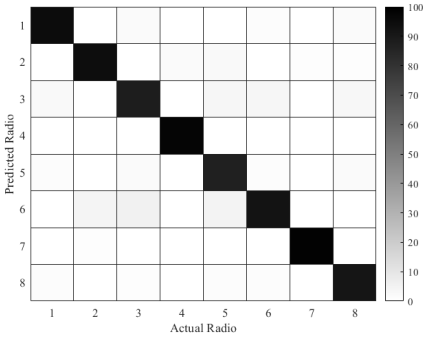

(h) SNR of 18 dB with an average accuracy of 92.99%.

Fig. 5. Confusion matrices showing percent correct classification performance for the eight IEEE 802.11a Wi-Fi radios. Each radio is represented by a set of 135×135 tiles, which are extracted from the grayscale image of a preamble's normalized, magnitude-squared GT representation. Tile selection is performed using entropy (ϵ, left-hand column) or entropy & mean ($\epsilon \& \mu$, right-hand column).

VI. Conclusion

This work assesses six entropy-based data reduction approaches applied to GT images–representing eight IEEE 802.11a Wi-Fi radios–to enhance IoT security via SEI. When compared to IQ only DL-based SEI, the entropy-based data reduction approach results in superior average percent correct classification performance for SNR values of 12 dB and higher while reducing the training time by over 75%. Future work will investigate modification of or additions to the presented approach in an attempt to improve SEI performance at lower SNR values.

References

[1] Chief Information Officer, U.S. Department of Defense, "DoD Policy Recommendations for The Internet of Things (IoT)," https://www.hsdl.org/?view&did=799676, Dec. 2016.

[2] Statista, "Internet of Things (IoT) connected devices installed base worldwide from 2015 to 2025 (in billions)," https://www.statista.com/statistics/471264/iot-number-of-connected-devices-worldwide/, 2019.

[3] K. Rawlinson, "HP Study Reveals 70 Percent of Internet of Things Devices Vulnerable to Attack," Jul 2014. [Online]. Available: https://www8.hp.com/us/en/hp-news/press-release.html?id=1744676

[4] I. Ray, D. Kar, J. Peterson, and S. Goeringer, "Device Identity and Trust in IoT-sphere Forsaking Cryptography," in *Int'l Conf on Collaboration and Internet Computing (CIC)*, 2019, pp. 204–213.

[5] N. Neshenko, E. Bou-Harb, J. Crichigno, G. Kaddoum, and N. Ghani, "Demystifying IoT Security: An Exhaustive Survey on IoT Vulnerabilities and a First Empirical Look on Internet-Scale IoT Exploitations," *IEEE Communications Surveys & Tutorials*, vol. 21, no. 3, pp. 1–32, 2019.

[6] F. Kandah, J. Cancelleri, D. Reising, A. Altarawneh, and A. Skjellum, "A Hardware-Software Co-design Approach to Identity, Trust, and Resilience for IoT/CPS at Scale," in *IEEE Int'l Conf on Internet of Things (iThings) and Green Computing and Communications (GreenCom) and Cyber, Physical and Social Computing (CPSCom) and Smart Data (SmartData)*, July 2019, pp. 1125–1134.

[7] D. Reising, J. Cancelleri, T. Loveless, F. Kandah, and A. Skjellum, "Radio Identity Verification-based IoT Security Using RF-DNA Fingerprints and SVM," *IEEE Internet of Things Journal*, pp. 8356–8371, 2020.

[8] Defense Advances Research Projects Agency (DARPA), "Spectrum Collaboration Challenge — Using AI to Unlock the True Potential of the RF Spectrum," https://archive.darpa.mil/sc2/, 2017.

[9] Y. Yu, T. Wang, and S. Liew, "Deep-reinforcement learning multiple access for heterogeneous wireless networks," in *Int'l Conf on Communications (ICC)*, 2018, pp. 1–7.

[10] T. O'Shea and J. Hoydis, "An Introduction to Deep Learning for the Physical Layer," *IEEE Trans on Cognitive Communications & Networking*, vol. 3, no. 4, pp. 563–575, Dec 2017.

[11] F. Restuccia and T. Melodia, "Polymorf: Polymorphic wireless receivers through physical-layer deep learning," in *Proceedings of the Twenty-First Int'l Symposium on Theory, Algorithmic Foundations, and Protocol Design for Mobile Networks and Mobile Computing*, ser. Mobihoc. Association for Computing Machinery, 2020, p. 271–280.

[12] Z. Qin, H. Ye, Y. Li, and B.-H. Juang, "Deep learning in physical layer communications," *IEEE Wireless Communications*, vol. 26, no. 2, pp. 93–99, 2019.

[13] J. Downey, B. Hilburn, T. O'Shea, and N. West, "In the Future, AIs—Not Humans—Will Design Our Wireless Signals," *IEEE Spectrum Magazine*, Apr 2020.

[14] M. Fadul, D. Reising, K. Arasu, and M. Clark, "Adversarial machine learning for enhanced spread spectrum communications," in *Military Communications Conf (MILCOM)*, 2021, pp. 783–788.

[15] F. Restuccia, S. D'Oro, A. Al-Shawabka, B. C. Rendon, S. Ioannidis, and T. Melodia, "DeepFIR: Channel-Robust Physical-Layer Deep Learning Through Adaptive Waveform Filtering," *IEEE Trans on Wireless Communications*, vol. 20, no. 12, pp. 8054–8066, 2021.

[16] M. Fadul, D. Reising, and M. Sartipi, "Identification of OFDM-Based Radios Under Rayleigh Fading Using RF-DNA and Deep Learning," *IEEE Access*, vol. 9, pp. 17 100–17 113, 2021.

[17] A. Al-Shawabka, F. Restuccia, S. D'Oro, T. Jian, B. Costa Rendon, N. Soltani, J. Dy, S. Ioannidis, K. Chowdhury, and T. Melodia, "Exposing the fingerprint: Dissecting the impact of the wireless channel on radio fingerprinting," in *IEEE Int'l Conf on Computer Communications (INFOCOM)*, 2020, pp. 646–655.

[18] S. Frank, "This AI can Spot an Art Forgery: With millions at stake, deep learning enters the art world," *IEE Spectrum*, Aug 2021.

[19] D. Reising, M. Temple, and J. Jackson, "Authorized and rogue device discrimination using dimensionally reduced RF-DNA fingerprints," *IEEE Trans on Information Forensics and Security*, vol. 10, no. 6, pp. 1180–1192, 2015.

[20] C. Wheeler and D. Reising, "Assessment of the impact of CFO on RF-DNA fingerprint classification performance," in *Int'l Conf on Computing, Networking and Communications (ICNC)*. IEEE, 2017, pp. 110–114.

[21] A. Wilson, D. Reising, and T. Loveless, "Integration of Matched Filtering within the RF-DNA Fingerprinting Process," in *IEEE Global Telecommunications Conf (GLOBECOM)*, 2019, pp. 1–6.

[22] P. Scanlon, I. Kennedy, and Y. Liu, "Feature extraction approaches to RF fingerprinting for device identification in femtocells," *Bell Labs Technical Journal*, vol. 15, no. 3, pp. 141–151, 2010.

[23] L. Sun, X. Wang, A. Yang, and Z. Huang, "Radio frequency fingerprint extraction based on multi-dimension approximate entropy," *IEEE Signal Processing Letters*, vol. 27, pp. 471–475, 2020.

[24] X. Wang, J. Duan, C. Wang, G. Cui, and W. Wang, "A radio frequency fingerprinting identification method based on energy entropy and color moments of the bispectrum," in *Int'l Conf on Advanced Infocomm Technology (ICAIT)*. IEEE, 2017, pp. 150–154.

[25] *IEEE Std 802.11-2007, Local and Metropolitan Area Networks, Part 11: Wireless LAN Medium Access Control (MAC) and Physical Layer (PHY) Specifications*, IEEE, Jun 2007.

[26] J. Tyler, M. Fadul, D. Reising, and E. Kaplanoglu, "Simplified denoising for robust specific emitter identification of preamble-based waveforms," in *Global Communications Conf (GLOBECOM)*. IEEE, 2021, pp. 1–7.

[27] J. Tyler, M. Fadul, D. Reising, and F. Kandah, "An Analysis of Signal Energy Impacts and Threats to Deep Learning Based SEI," in *IEEE Int'l Conf on Communications (ICC)*, Jun 2022.

[28] WiSilica, "Top 6 IoT Communication Protocols," https://wisilica.com/company/top-6-iot-communication-protocols/, Aug. 2020.

[29] H. Lajos, A. Yosef, W. Li, and J. Ming, *MIMO-OFDM for LTE, Wi-Fi, and WiMAX*. John Wiley & Sons, Ltd., 2011.

[30] M. Bastiaans and M. Geilen, "On the discrete Gabor transform and the discrete Zak transform," *Signal processing*, vol. 49, no. 3, pp. 151–166, 1996.

[31] D. Reising, M. Temple, and M. Oxley, "Gabor-based RF-DNA fingerprinting for classifying 802.16e WiMAX Mobile Subscribers," in *Int'l Conf on Computing, Networking and Communications (ICNC)*, 2012, pp. 7–13.

[32] T. Schmidl and D. Cox, "Robust frequency and timing synchronization for OFDM," *IEEE Trans on Communications*, vol. 45, no. 12, pp. 1613–1621, 1997.

[33] R. Gonzalez, R. Woods, and S. Eddins, *Digital Image Processing Using MATLAB*. New Jersey, Prentice Hall, 2003.

[34] A. Prügel-Bennett, *The Probability Companion for Engineering and Computer Science*. Cambridge University Press, 2020.

[35] T. Hastie, R. Tibshirani, J. H. Friedman, and J. H. Friedman, *The elements of statistical learning: data mining, inference, and prediction*. Springer, 2009, vol. 2.

[36] MATLAB, *version 9.9.0.1462360 (R2020b)*. Natick, Massachusetts: The MathWorks Inc., 2020.

[37] C. Shorten and T. M. Khoshgoftaar, "A survey on image data augmentation for deep learning," *Journal of big data*, vol. 6, no. 1, pp. 1–48, 2019.